PERGAMON

Journal of Structural Geology 25 (2003) 277–289

JOURNAL OF STRUCTURAL GEOLOGY

www.elsevier.com/locate/jsg

How to calculate normal curvatures of sampled geological surfaces

Stephan Bergbauer*, David D. Pollard

Department of Geological and Environmental Sciences, Stanford University, Stanford, CA 94305, USA

Received 16 January 2001; accepted 17 October 2001

Abstract

Curvature has been used both to describe geological surfaces and to predict the distribution of deformation in folded or domed strata. Several methods have been proposed in the geoscience literature to approximate the curvature of surfaces; however we advocate a technique for the exact calculation of normal curvature for single-valued gridded surfaces. This technique, based on the First and Second Fundamental Forms of differential geometry, allows for the analytical calculation of the magnitudes and directions of principal curvatures, as well as Gaussian and mean curvature. This approach is an improvement over previous methods to calculate surface curvatures because it avoids common mathematical approximations, which introduce significant errors when calculated over sloped horizons. Moreover, the technique is easily implemented numerically as it calculates curvatures directly from gridded surface data (e.g. seismic or GPS data) without prior surface triangulation.

In geological curvature analyses, problems arise because of the sampled nature of geological horizons, which introduces a dependence of calculated curvatures on the sample grid. This dependence makes curvature analysis without prior data manipulation problematic. To ensure a meaningful curvature analysis, surface data should be filtered to extract only those surface wavelengths that scale with the feature under investigation. A curvature analysis of the top-Pennsylvanian horizon at Goose Egg dome, Wyoming shows that sampled surfaces can be smoothed using a moving average low-pass filter to extract curvature information associated with the true morphology of the structure.

Keywords: Curvature; Surfaces; Geologic structure

1. Introduction

The normal curvature is an inherent property of surfaces deducible from geological or geophysical field measurements independent of the reference frame. In the geological context the surface may be the top or bottom of a sedimentary formation, member, or bed. Curvature analysis of geological surfaces has been employed to describe the geometry of strata (e.g. Bevis, 1986; Lisle, 1992; Lisle and Robinson, 1995; Ansell and Bannister, 1996; Roberts, 2001), to quantify the degree of deformation or strain in deformed strata (e.g. Ekman, 1988; Lisle, 1994; Nothard et al., 1996; Samson and Mallet, 1997; Johnson and Johnson, 2000; Roberts, 2001), and to predict fracture orientations and densities of bent or folded strata (e.g. Murray, 1968; Thomas et al., 1974; Lisle, 1994; Fischer and Wilkerson, 2000; Hennings et al., 2000). Whereas some authors concluded curvature analysis is a valid tool for predicting deformation (e.g. Ewy and Hood, 1984; Lisle, 1994) others doubt the predictive capability of such analyses (e.g. Schultz-Ela and Yeh, 1992; Gibbs et al., 1997; Jamison, 1997).

Some investigators have been challenged by the task of calculating surface curvature (e.g. Schultz-Ela and Yeh, 1992). Often, the second partial derivative of the surface (rate of dip change, sometimes referred to as structural curvature) is calculated and used as a proxy for curvature (e.g. Murray, 1968; Turcotte and Schubert, 1982; Ericsson et al., 1998; Fischer and Wilkerson, 2000; Johnson and Johnson, 2000). Others have estimated curvature not of the surface, but along the coordinate lines of an arbitrarily chosen global coordinate system (e.g. Murray, 1968; Ivanov, 1989; Nothard et al., 1996; Stewart and Wynn, 2000). In most of these cases, however, the directions of minimum and maximum surface curvature do not coincide with the coordinate directions. Techniques for finding the magnitudes and directions of principal surface curvature utilize approximations that are not necessarily reliable (e.g. Lisle and Robinson, 1995; Stewart and Podolski, 1998; Fischer and Wilkerson, 2000).

The geologist, concerned with the estimation of a horizon's curvature, will find a wealth of proposed methods in the geoscience literature on how to calculate the curvature

* Corresponding author.
E-mail address: stephan@pangea.stanford.edu (S. Bergbauer).

0191-8141/02/$ - see front matter © 2002 Published by Elsevier Science Ltd.
PII: S0191-8141(02)00019-6

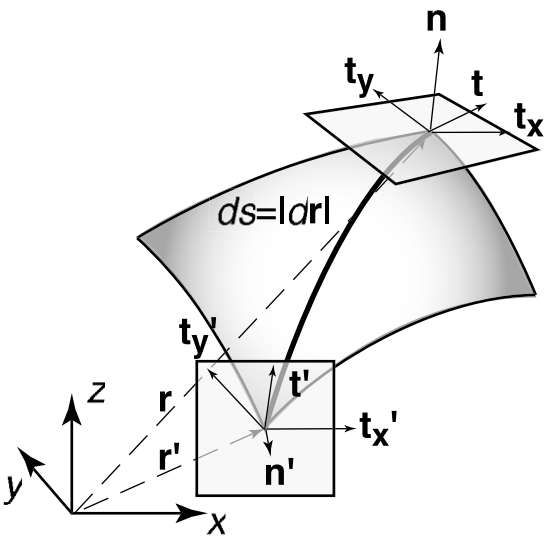

Fig. 1. The curvature of an arbitrary surface is defined as the rate of change of tangent vector **t** as one moves along the arc of a curve d*s* on the surface (thick curved line). The vector **n** is the unit normal to the surface at the point defined by the position vector **r**. $\mathbf{t}_y$ and $\mathbf{t}_x$ are tangent vectors that define the tangent plane at this point.

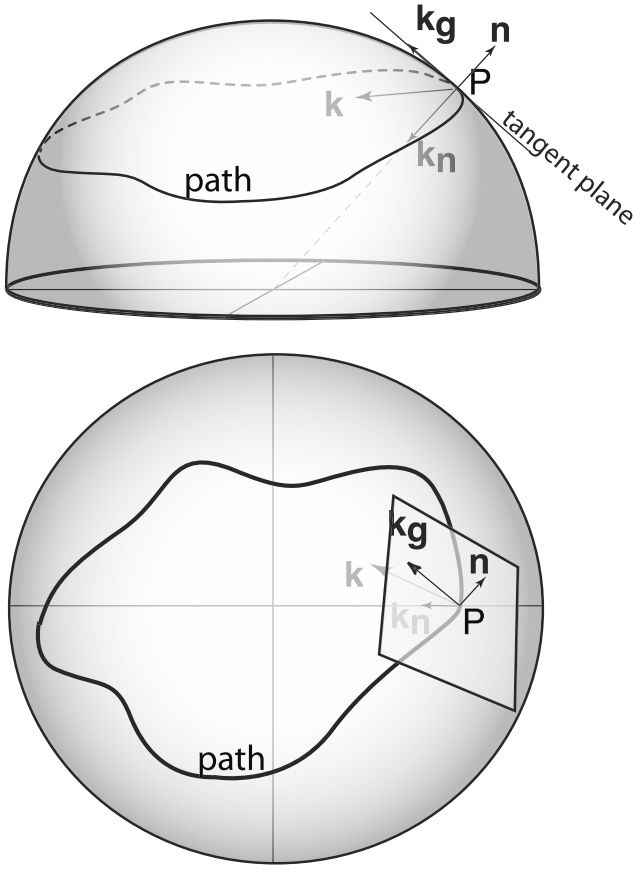

Fig. 2. The curvature vector **k** at the point P is composed of vectors normal ($\mathbf{k}_n$) and tangential ($\mathbf{k}_g$) to the surface. The normal curvature vector parallels the normal vector **n** and points toward the center of curvature of the surface, whereas the tangential curvature vector points toward the center of curvature of the path in the tangential plane. The magnitude of $\mathbf{k}_n$ is a function of the curvature of the surface, whereas the magnitude of $\mathbf{k}_g$ depends on the amount of 'meandering' of the path on the surface.

of a surface (e.g. Murray, 1968; Ekman, 1988; Ivanov, 1989; Schultz-Ela and Yeh, 1992; Lisle, 1994; Lisle and Robinson, 1995; Nothard et al., 1996; Samson and Mallet, 1997; Stewart and Podolski, 1998; Fischer and Wilkerson, 2000; Johnson and Johnson, 2000; Roberts, 2001). Even though the normal surface curvature is an invariant property of a surface, each of these techniques provides a different estimate of curvature. We present a derivation of the expressions for calculating the normal surface curvature from the fundamental forms of surfaces in the geological context. The technique we present is the mathematically precise way of calculating the curvature of a sampled surface, and other techniques proposed in the geoscience literature are approximations or simplifications of what is presented here. It is beyond the scope of this paper to compare this exact technique with every approximate solution; however, we do compare this method with one of the 'second partial derivative' methods. More complete derivations of the fundamental forms and surface curvature can be found in introductory books on *differential geometry* (e.g. Struik, 1961; Stoker, 1969; Nutbourne and Martin, 1988).

The fact that an exact mathematical expression usually cannot be established for geological surfaces poses a problem for the calculation of surface curvature. Geological surfaces are represented by discretely sampled data (e.g. seismic, GPS, total station), and issues inherent to sampled data such as grid spacing, smoothing, and data aliasing need to be addressed (Schultz-Ela and Yeh, 1992; Stewart and Podolski, 1998; Stewart and Wynn, 2000). The results presented here show that calculating surface curvature over non-smoothed data sets may lead to questionable, and perhaps uninterpretable results, thus arguing for the necessity to manipulate these data prior to curvature calculation. We present one effective smoothing technique for surface data prior to curvature analysis and show how it adds meaning to the curvature analysis of the top-Pennsylvanian at Goose Egg Dome, Wyoming (Harris et al., 1960). This paper is not intended to provide an analysis of the different techniques available for the smoothing of data; rather we would like to emphasize the necessity for sensible data manipulation prior to curvature calculation. Moreover, since the quality of a surface representation depends on the density of the sample grid, the resolvable surface curvatures are also limited by the grid spacing used to sample the surface. If, for example, one chooses to calculate bending strains from these curvatures, the limitations introduced by the sample grid should be acknowledged.

2. Definition of curvature

The curvature of a surface is defined in terms of the curvature of an arbitrary line that lies in that surface. The

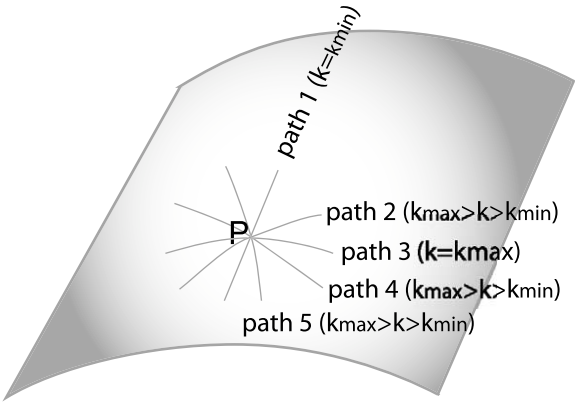

Fig. 3. The magnitude of the normal surface curvature at point P depends on the direction of the path (gray lines) through point P. At every point P on the surface there are two orthogonal directions (paths 1 and 3) in which the normal curvature magnitudes assume extreme values: the principal curvature directions. Normal curvature magnitudes calculated in any other direction at P will fall between these two principal values.

curvature of a line equals the change of the tangent vector (**t**) as one proceeds a differential distance (d*s*) along the line (Fig. 1). The arc length d*s* equals the absolute value of the difference (d**r**) of position vectors **r** and **r**′ defining the two endpoints of the arc. As one proceeds over a curved surface along a meandering path, the direction of the path with respect to a global coordinate changes for two reasons: first because the surface is curved, and second because the path meanders over the surface. Thus the curvature vector (**k**) is composed of two vectors, one normal to the surface, and the second lying in the tangent plane to the surface (Eq. 5-2 in Chapter 2 of Struik, 1961):

$$\mathrm{d}\mathbf{t}/\mathrm{d}s = \mathbf{k} = \mathbf{k}_\mathrm{n} + \mathbf{k}_\mathrm{g}, \tag{1}$$

where $\mathbf{k}_\mathrm{n}$ is the *normal curvature vector*, and $\mathbf{k}_\mathrm{g}$ is the *geodesic* (or *tangent*) *curvature vector* (Fig. 2). The normal curvature vector points toward the center of curvature of the surface, and its magnitude is the *normal surface curvature*. On a sphere, for example, the value of the normal curvature remains constant and the vector points to the center of the sphere from any point on the surface, independent of the path taken over the surface. The geodesic curvature vector, in contrast, lies in the tangent plane to the surface at point P and is a measure of the meandering of the path across the surface. On a sphere, for example, the magnitude of the geodesic curvature is not necessarily constant and will change depending on the path taken across the sphere. Focusing only on evaluating the normal curvature vector is therefore sufficient to describe the curvature of the surface itself.

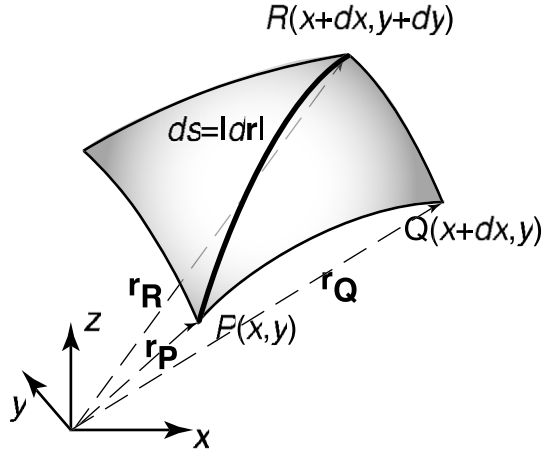

Fig. 4. The arc length d*s* between two points P and R on a surface can be expressed in terms of the vectors $\mathbf{r}_\mathrm{P}$, $\mathbf{r}_\mathrm{Q}$ and $\mathbf{r}_\mathrm{R}$. The First Fundamental Form follows directly from the square of the arc length.

Normal surface curvature is calculated along paths across the surface. For surfaces other than a sphere, the normal curvature depends on the direction of the path in which it is calculated. For the cylindrical fold shown in Fig. 3, the normal surface curvature is zero along the fold axis and maximum in the direction perpendicular to the fold axis. Because there are an infinite number of possible directions that cross a point P on a surface, there are an infinite number of normal surface curvatures one could evaluate. The magnitude of the calculated normal curvature vector at this point will vary depending on the path taken through the point P, but the direction of this vector is always parallel to the unit normal vector **n** on the surface at P. There are two orthogonal directions at P in which the normal curvature takes on extreme values, called the *principal surface curvatures*. All other curvature values at P fall between these two extreme values. Normal surface curvatures can be calculated in any direction, for example along strike or dip of the surface (Roberts, 2001).

3. Calculating the normal surface curvature

3.1. First Fundamental Form

In 3-D Euclidean space, a surface is sufficiently described by two quadratic differential equations, the so-called *First and Second Fundamental Forms*. The normal surface curvature can be calculated from these two fundamental forms. The First Fundamental Form follows directly from the Pythagorean representation of a differential arc length d*s* on the surface (Fig. 4). The arc length d*s* between the points P and R on a surface can be expressed in terms of the position vectors $\mathbf{r}_\mathrm{Q}$, $\mathbf{r}_\mathrm{P}$, and $\mathbf{r}_\mathrm{R}$. The square of d*s* is related to these vectors as:

$$\mathrm{d}s^2 = \mathrm{d}\mathbf{r}^2 = (\mathbf{r}_\mathrm{PQ} + \mathbf{r}_\mathrm{QR})^2 = \mathbf{r}_\mathrm{PQ}\cdot\mathbf{r}_\mathrm{PQ} + 2\mathbf{r}_\mathrm{PQ}\cdot\mathbf{r}\mathrm{QR} + \mathbf{r}_\mathrm{QR}\cdot\mathbf{r}_\mathrm{QR}. \tag{2}$$

Here

$$\mathbf{r}_\mathrm{PQ} = \mathbf{r}_\mathrm{Q} - \mathbf{r}_\mathrm{P}$$

and

$$\mathbf{r}_{QR} = \mathbf{r}_R - \mathbf{r}_Q$$

are the distances between points P and Q, and points Q and R, respectively, and the dot indicates the scalar product of two vectors. In vector notation, a surface can be expressed as:

$$\mathbf{r}(x,y) = x\mathbf{e}_x + y\mathbf{e}_y + z(x,y)\mathbf{e}_z, \tag{3}$$

where $\mathbf{r}$ is the position vector of every point on the surface, x and y are two independent parameters, $z(x,y)$ is an elevation measurement with respect to the x–y parameter plane, and $\mathbf{e}_x$, $\mathbf{e}_y$, and $\mathbf{e}_z$ are the unit vectors in the direction of the Cartesian coordinate system axes. The vectors defining ds in Eq. (2) can be expressed using Eq. (3):

$$\mathbf{r}_{PQ} = x_Q\mathbf{e}_x + y_Q\mathbf{e}_y + z_Q(x,y)\mathbf{e}_z - [x_P\mathbf{e}_x + y_P\mathbf{e}_y + z_P(x,y)\mathbf{e}_z],$$

$$\mathbf{r}_{QR} = x_R\mathbf{e}_x + y_R\mathbf{e}_y + z_R(x,y)\mathbf{e}_z - [x_Q\mathbf{e}_x + y_Q\mathbf{e}_y + z_Q(x,y)\mathbf{e}_z].$$

Using the coordinates of the points P, Q, and R as shown in Fig. 4, the partial derivatives (slopes of the surface) in the directions of the two parameters are (in the limit as dx and dy go to zero):

$$\frac{\partial z}{\partial x} = \frac{z_Q - z_P}{\mathrm{d}x}$$

and

$$\frac{\partial z}{\partial y} = \frac{z_R - z_Q}{\mathrm{d}y}.$$

Eq. (2) can now be recast as (Eq. 5-8 in Chapter 2 of Struik, 1961):

$$\mathrm{I} = \mathrm{d}s^2 = \mathrm{d}\mathbf{r}^2 = \alpha_{xx}\mathrm{d}x^2 + 2\alpha_{xy}\mathrm{d}x\mathrm{d}y + \alpha_{yy}\mathrm{d}y^2, \tag{4a}$$

where

$$\alpha_{xx} = 1 + \left(\frac{\partial z}{\partial x}\right)^2,\ \alpha_{xy} = \left(\frac{\partial z}{\partial x}\right)\cdot\left(\frac{\partial z}{\partial y}\right),\ \text{and}\ \alpha_{yy} = 1 + \left(\frac{\partial z}{\partial y}\right)^2. \tag{4b}$$

α_{xx}, α_{xy}, and α_{yy} are called the *metric coefficients* of the surface (Eq. 2-7 in Chapter 2 of Struik, 1961). Eqs. (4a) and (4b) is called the First Fundamental Form of surfaces (I). Since the First Fundamental Form is the square of an arc length ds, the First Fundamental Form is always positive. This fundamental form provides a basis for a metric representation of distances, angles, and areas on a surface. Considering that the arc length between two points on a surface is constant regardless of the coordinate system in which it is measured, the First Fundamental Form is invariant with respect to coordinate transformation.

3.2. Second Fundamental Form

The Second Fundamental Form describes the spatial rate of change of the unit normal vector $\mathbf{n}$ to a surface and the spatial rate of change of position on that surface (d$\mathbf{n}$·d$\mathbf{r}$). As shown in Fig. 1, the unit normal vector $\mathbf{n}$ at a point is perpendicular to the tangent plane at this point. The tangent plane is defined by two tangent vectors that point in the directions defined by the parameters x and y, respectively (Eq. 3-1 in Chapter 2 of Struik, 1961):

$$\mathbf{t}_x = \frac{\partial \mathbf{r}}{\partial x} = \mathbf{e}_x + \left(\frac{\partial z}{\partial x}\right)\mathbf{e}_z$$

and

$$\mathbf{t}_y = \frac{\partial \mathbf{r}}{\partial y} = \mathbf{e}_y + \left(\frac{\partial z}{\partial y}\right)\mathbf{e}_z.$$

The unit normal vector $\mathbf{n}$ to the tangent plane is given by the cross product of these two tangent vectors divided by the magnitude of this product (Eq. 3-2 in Chapter 2 of Struik, 1961):

$$\mathbf{n} = \frac{\mathbf{t}_x \times \mathbf{t}_y}{\left|\mathbf{t}_x \times \mathbf{t}_y\right|} = \frac{\mathbf{e}_z - \dfrac{\partial z}{\partial x}\mathbf{e}_x - \dfrac{\partial z}{\partial y}\mathbf{e}_y}{\sqrt{\alpha_{xx}\alpha_{yy} - \alpha_{xy}^2}}. \tag{5}$$

Using Eqs. (3) and (5), d$\mathbf{n}$ and d$\mathbf{r}$ are defined by their total derivatives:

$$\mathrm{d}\mathbf{n} = \frac{\partial \mathbf{n}}{\partial x}\mathrm{d}x + \frac{\partial \mathbf{n}}{\partial y}\mathrm{d}y$$

and

$$\mathrm{d}\mathbf{r} = \frac{\partial \mathbf{r}}{\partial x}\mathrm{d}x + \frac{\partial \mathbf{r}}{\partial y}\mathrm{d}y.$$

The Second Fundamental Form can be written as (Eq. 5-8 in Chapter 2 of Struik, 1961):

$$\mathrm{II} = -\mathrm{d}\mathbf{n}\cdot\mathrm{d}\mathbf{r} = \beta_{xx}\mathrm{d}x^2 + 2\beta_{xy}\mathrm{d}x\mathrm{d}y + \beta_{yy}\mathrm{d}y^2, \tag{6a}$$

with

$$\beta_{xx} = \frac{\dfrac{\partial^2 z}{\partial x^2}}{\sqrt{\alpha_{xx}\alpha_{yy} - \alpha_{xy}^2}},\ \beta_{xy} = \frac{\dfrac{\partial^2 z}{\partial x \partial y}}{\sqrt{\alpha_{xx}\alpha_{yy} - \alpha_{xy}^2}},\ \textit{and}\ \beta_{yy} = \frac{\dfrac{\partial^2 z}{\partial y^2}}{\sqrt{\alpha_{xx}\alpha_{yy} - \alpha_{xy}^2}}, \tag{6b}$$

the coefficients of the Second Fundamental Form (Eq. 5-10 in Chapter 2 of Struik, 1961). These coefficients are sometimes called the curvature coefficients, as they, in conjunction with the metric coefficients, provide information about the deviation of the surface from its tangent plane. The Second Fundamental Form is also invariant with respect to coordinate transformation.

3.3. Normal surface curvature

The magnitude of the normal curvature of a surface is calculated by dividing the two fundamental forms. From

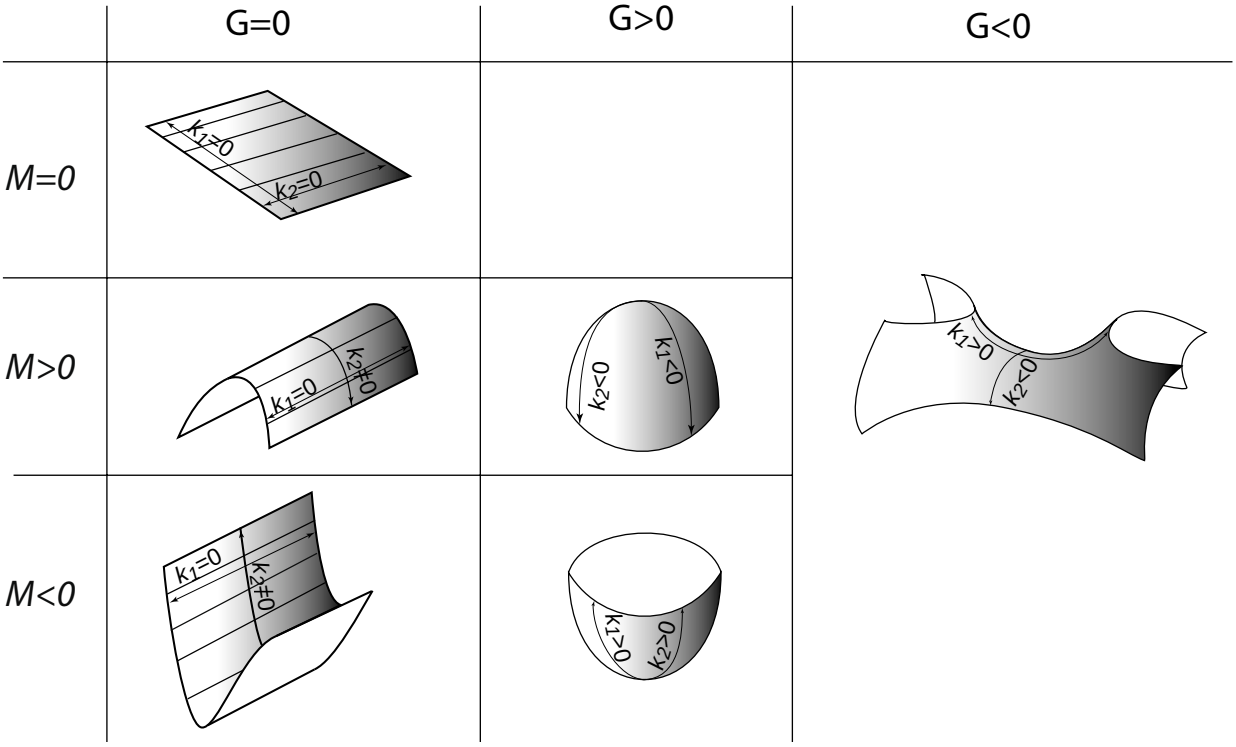

Fig. 5. Gaussian curvature (G) and mean curvature (M) are well suited to infer the shape of surfaces. G equals zero for cylindrical points on surfaces, such as points on cylindrical anticlines ($M > 0$), cylindrical synclines ($M < 0$), and planes ($M = 0$). G is positive in value for basins ($M < 0$) and domes ($M > 0$), and is negative for saddle points.

Eqs. (4a), (4b), (6a) and (6b) it follows (Eq. 5-6 in Chapter 2 of Struik, 1961):

$$k_n = \frac{\mathrm{II}}{\mathrm{I}} = \frac{\beta_{xx}\mathrm{d}x^2 + 2\beta_{xy}\mathrm{d}x\mathrm{d}y + \beta_{yy}\mathrm{d}y^2}{\alpha_{xx}\mathrm{d}x^2 + 2\alpha_{xy}\mathrm{d}x\mathrm{d}y + \alpha_{yy}\mathrm{d}y^2}. \tag{7}$$

This equation shows that different normal surface curvature magnitudes k_n are calculated for different directions taken through the point of interest by varying dx and dy. k_n is also an invariant property of a surface. Eq. (7) reduces to the standard formula for calculating the curvature at points along a curved line lying in the (x,z)-plane that can be found in most books on calculus (e.g. Stewart, 1995):

$$k_x = \frac{\dfrac{\partial^2 z}{\partial x^2}}{\left[1 + \left(\dfrac{\partial z}{\partial x}\right)^2\right]^{3/2}}. \tag{8}$$

This is the form of the equation cited by Murray (1968), Ivanov (1989), Nothard et al. (1996), and Stewart and Podolski (1998) and referred to as *the* curvature, but it is a very special case of the normal surface curvature.

3.4. Principal curvature directions

Relative to the arbitrarily chosen differential parameters dx and dy, two orthogonal directions can be found in the tangent plane in which the normal curvature obtains extreme values (the principal curvatures of a surface, k_1 and k_2). By dividing by dx^2, Eq. (7) can be recast as (Eq. 6-3 in Chapter 2 of Struik, 1961):

$$k_{n(\lambda)} = \frac{\mathrm{II}}{\mathrm{I}} = \frac{\beta_{xx} + 2\beta_{xy}\lambda + \beta_{yy}\lambda^2}{\alpha_{xx} + 2\alpha_{xy}\lambda + \alpha_{yy}\lambda^2} \tag{9}$$

where $\lambda = \mathrm{d}y/\mathrm{d}x$. The principal directions λ_1 and λ_2 (lines of curvature) are found by solving:

$$\frac{\partial k_n(\lambda)}{\partial \lambda} = 0.$$

It follows that:

$$\lambda_{1,2} = -\frac{\alpha_{xx}\beta_{yy} - \alpha_{yy}\beta_{xx}}{2(\alpha_{xy}\beta_{yy} - \alpha_{yy}\beta_{xy})} \pm \frac{\sqrt{\dfrac{1}{4}(\alpha_{xx}\beta_{yy} - \alpha_{yy}\beta_{xx})^2 - (\alpha_{xy}\beta_{yy} - \alpha_{yy}\beta_{xy})(\alpha_{xx}\beta_{xy} - \alpha_{xy}\beta_{xx})}}{\alpha_{xy}\beta_{yy} - \alpha_{yy}\beta_{xy}}. \tag{10}$$

3.5. Principal curvature magnitudes

Once the principal directions λ_1 and λ_2 are found by solving Eq. (10), the magnitude of the principal curvatures k_1 and k_2 can be calculated by substituting λ_1 and λ_2 into Eq. (9).

3.6. Gaussian and mean curvature

The Gaussian curvature G (Gauss, 1827) is defined as the product of the two principal curvatures (Eq. 7-3 in Chapter 2 of Struik, 1961):

$$G = k_1 \cdot k_2 = \frac{\beta_{xx}\beta_{yy} - \beta_{xy}^2}{\alpha_{xx}\alpha_{yy} - \alpha_{xy}^2}. \quad (11)$$

Gaussian curvature is one of the two important quantities that are useful for surface description (Fig. 5). If the Gaussian curvature equals zero, then at least one of the principal curvatures has to equal zero, in which case the surface is cylindrically shaped (Fig. 5). In cases where both principal curvatures are zero, the surface is a plane. If $G < 0$, then the sign of the two principal curvatures are opposite, and the surface forms a saddle (Fig. 5). If $G > 0$, then the two principal curvatures have the same sign, and the surface at this point will have a local extremum. Therefore, the surface will either be shaped like a dome or a bowl (Fig. 5).

Surfaces with equal Gaussian curvature can be distinguished based on a second important quantity, namely the mean curvature (M) (Roberts, 2001). For example, for zero Gaussian curvature the cylindrical surface could be either flat ($M = 0$), or shaped like a cylindrical anticline ($M > 0$), or a cylindrical syncline ($M < 0$). Similarly, for surfaces with positive Gaussian curvatures, the mean curvature can distinguish between a dome ($M > 0$) and a bowl ($M < 0$). The mean curvature can be calculated in terms of the principal normal curvatures or using the coefficients of the fundamental forms (Eq. 7-2 in Chapter 2 of Struik, 1961):

$$M = \frac{1}{2}(k_1 + k_2) = \frac{\alpha_{11}\cdot\beta_{22} + \beta_{11}\cdot\alpha_{22} - 2\cdot\alpha_{12}\cdot\beta_{12}}{2(\alpha_{11}\cdot\alpha_{22} - \alpha_{12}^2)}. \quad (12)$$

In this way we understand that Gaussian and mean curvatures are necessary quantities to describe the general shapes of surfaces in terms of the fundamental forms. Gaussian curvature alone is not sufficient for this purpose.

3.7. Developable surfaces

A developable surface can be thought of as one that can be unfolded to a flat surface without having to cut or stretch the surface. Surfaces like cones, cylinders, and planes are developable surfaces. A necessary and sufficient condition for a surface to be developable is that its Gaussian curvature be zero everywhere. This condition is only achieved when the numerator of Eq. (11) equals zero. In other words, a developable surface is a surface for which at least one principal curvature is zero everywhere.

It is important to note that $G = 0$ is not a sufficient condition for a surface to be un-stretched or un-sheared. The Gaussian curvature of a planar surface that has been stretched or sheared in its plane still equals zero. Furthermore, the surfaces of a layer with finite thickness deformed into a cylindrical fold are stretched despite a zero Gaussian curvature. Thus Gaussian curvature by itself, despite the suggestion of Lisle (1994), is unsuited for evaluating the state of deformation within surfaces.

4. Comparison of this method with existing techniques

4.1. Triangulation methods

In 1992, Schultz-Ela and Yeh evaluated existing methods to calculate surface curvature and concluded that they needed improvement. Apparently, this problem has persisted as indicated by Stewart and Wynn (2000), who point out that only simple surfaces can be analyzed with the existing curvature algorithms. The method presented here to compute normal curvature over arbitrarily sampled surfaces is mathematically accurate and can be applied to any single valued surface description without having to triangulate a surface from the data points prior to curvature analysis. Any gridded surface data, such as horizon depth data from seismic surveys or surface elevations recorded using GPS, can be used directly without having to numerically construct the surface prior to curvature calculation.

Surface triangulation algorithms construct a surface from discrete data points and subsequently the resulting surface geometry depends on the method used for triangulation. Surfaces using the GOCAD® approach are triangulated by fitting Bezier patches over several discrete data points by minimizing the distance between the patch and each data point the patch covers (Mallet, 1992). This triangulation is dependent on the parameterization used, which affects calculated curvatures (Samson and Mallet, 1997). With the technique presented here, the surface does not need to be constructed as the curvature can be calculated directly from the sample grid. This not only removes the additional ambiguity introduced by the triangulation method, but the method presented here does not require the availability of software packages such as GOCAD® to calculate surface curvatures. In addition to relying on triangulated surfaces, the angular defect method (Calladine, 1986; Lisle, 1994) is limited to calculating Gaussian curvature.

Other existing methods that, like the method presented here, allow for the calculation of curvatures directly from the gridded data without prior triangulation have used only the second partial surface derivative as a proxy for the true normal surface curvature. This approximation, however, introduces significant errors when applied to sloping surfaces. None of these limitations apply to the method presented here, and the accuracy of the calculated curvature only depends on the accuracy with which the first (slope) and second (change of slope) partial derivatives can be evaluated. Any standard numerical techniques can be employed to calculate the derivatives; we use the finite differences method (Ames, 1992) making the numerical implementation of this method straightforward.

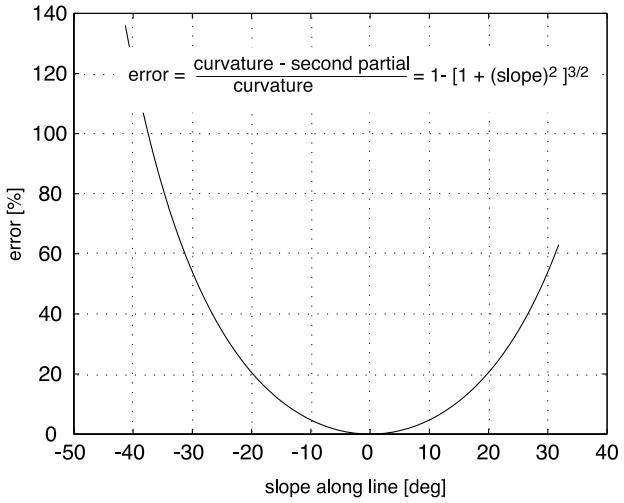

Fig. 6. The error between the absolute value of curvature of a planar curve and the second partial derivative as a function of slope along the curved line. Using the second partial derivative as an approximation for curvature of surfaces with slopes greater than 30°, an error of 50% is introduced.

4.2. Second partial derivative methods in 1-D

The second partial derivative of a surface has been used, and is still being used, as a proxy for curvature (e.g. Murray, 1968; Pollard and Johnson, 1973; Turcotte and Schubert, 1982; Ericsson et al., 1998; Jackson and Pollard, 1988; Fischer and Wilkerson, 2000; Johnson and Johnson, 2000). These investigators argue, based on Eq. (8), that for small surface slopes the error introduced by this simplification is small. By introducing this simplification, however, one not only accepts errors in the magnitude of curvature, but also in the locations of the extreme values and in the directions of the principal curvatures.

The error between calculated curvature of a planar curve and the second partial derivative can be investigated analytically using Eq. (8), which consists of a slope and a change of slope term. The error between curvature and second partial derivative magnitudes is a function of the slope and assumes the following form:

$$\text{error}\,[\%] = 1 - \left[1 + \left(\frac{\partial z}{\partial x}\right)^2\right]^{3/2} \times 100. \tag{13}$$

Fig. 6 depicts the error in percent as a function of the slope of the line. The error between curvature and the second partial derivative is small where the slope of the surface is small; however, it increases rapidly as the slope increases. Considering that geological surfaces, such as domes and folds, often exhibit slopes of 30° or greater, the error accepted when using the second partial derivative as a proxy for curvature can be greater than 50%.

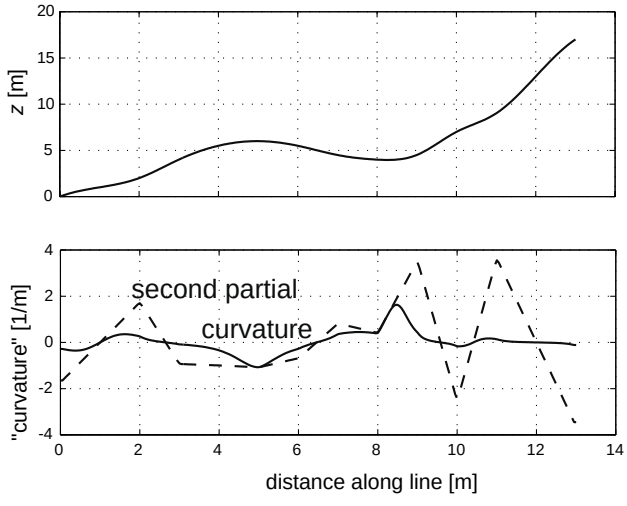

Fig. 7. Comparison of calculated curvature according to Eq. (8) (solid line, lower) and the second partial derivative (dashed line, lower) along an arbitrary line (upper). The locations of the extreme values of both 'measures of curvature' do not coincide, and magnitudes are different.

Fig. 7 depicts an arbitrary line (upper plot) sampled every 5 cm for which the second partial derivative (dashed line in lower plot) and the curvature according to Eq. (8) (solid line in lower plot) have been calculated. The figure demonstrates that not only are the absolute values of the two measures of 'curvature' different, but the locations of the extreme values of both measures of curvature do not coincide.

4.3. Second partial derivative methods in 2-D

When dealing with a surface, several techniques have been proposed for calculating the principal directions of curvature. Timoshenko and Woinowsky-Krieger (1959), for example, use the assumption of small deflections of thin plates to derive expressions for the principal surface curvatures and their directions as a function of the second partial derivative only:

$$k_n = -\frac{\partial^2 z}{\partial x^2}\cos^2\alpha - \frac{\partial^2 z}{\partial x \partial y}\sin 2\alpha - \frac{\partial^2 z}{\partial y^2}\sin^2\alpha, \tag{14a}$$

where

$$\alpha_{1,2} = \frac{1}{2}\tan^{-1}\left[-2\left(\frac{\dfrac{\partial^2 z}{\partial x \partial y}}{\dfrac{\partial^2 z}{\partial x^2} - \dfrac{\partial^2 z}{\partial y^2}}\right)\right] \tag{14b}$$

are the principal directions. This concept for calculating principal curvatures is applied by Fischer and Wilkerson (2000) to a model of a geological fold dipping up to 30°. Schultz-Ela and Yeh (1992) discuss several methods for calculating surface curvatures, favoring the 'ring method' and the 'scalar second derivative method' over the 'gradient second derivative method'. Ericsson et al. (1998) use the rate of dip change measured in the direction of maximum dip as the structural curvature.

Evaluating the mismatch between each of these methods and the true normal curvature is beyond the scope of this paper. However, a comparison of this method with the method used by Fischer and Wilkerson (2000) is presented

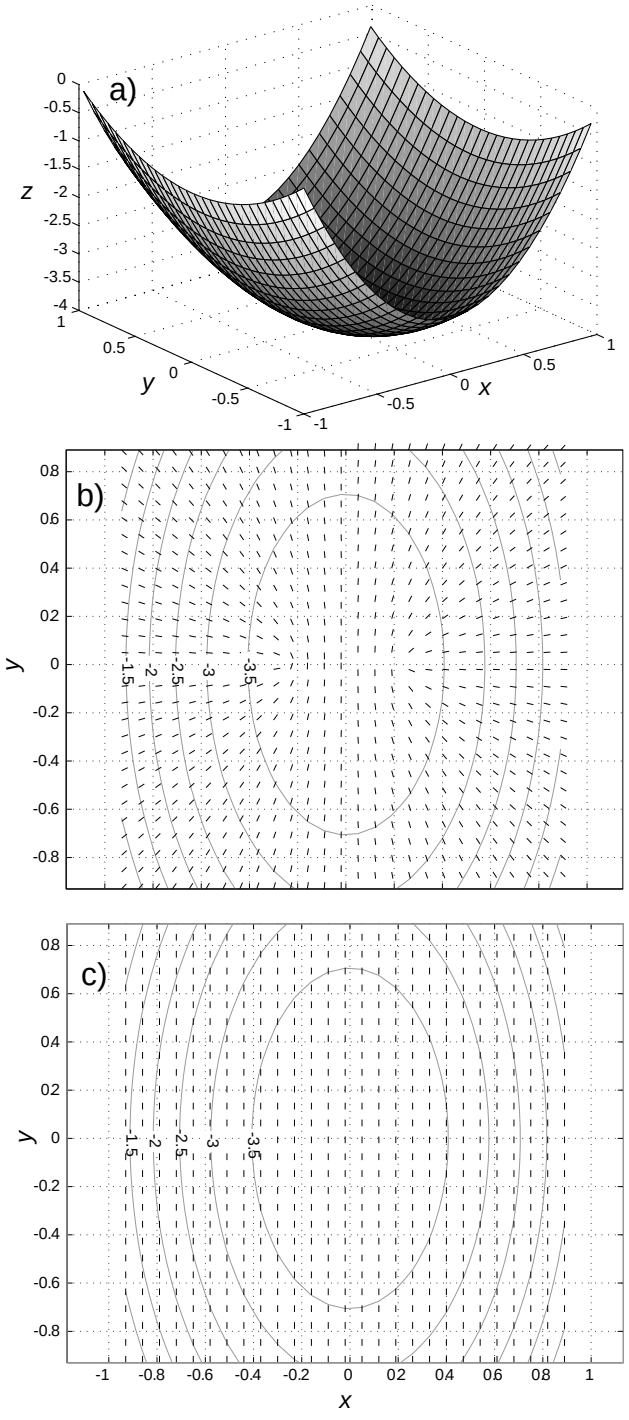

Fig. 8. Comparison of exact directions of minimum curvature and approximate directions based on the assumption of thin plate theory for an analytical basin. (a) 3-D representation of basin topography, (b) directions of exact minimum curvature for the surface shown by tick marks, and (c) directions of approximate minimum curvature calculated using thin plate theory. Gray contours in (b) and (c) show the topography of the surface. The mismatch between the two solutions vanishes only along $x = 0$. If joints formed as Fischer and Wilkerson (2000) hypothesize, they would parallel the direction of minimum curvature.

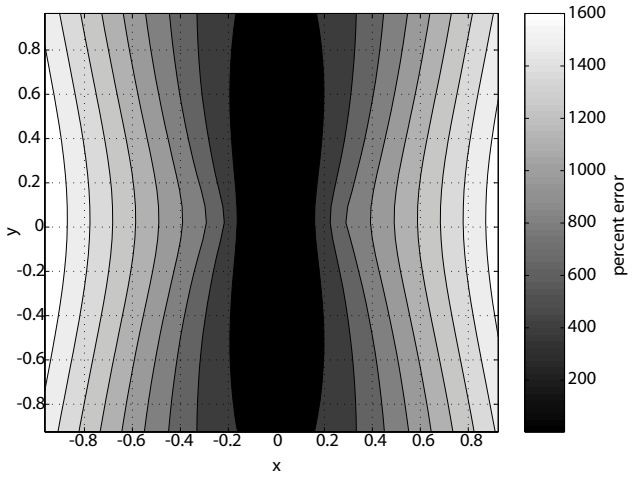

Fig. 9. Error [%] between exact maximum curvature and the approximate value based on the assumption of thin plate theory for the surface of Fig. 8. The error is small near the center of the basin where the slope is small, however, the error exceeds 50% for slopes greater than about 30°. The error exceeds several hundred percent for the steep part of the surface.

as an example. For an idealized basin (Fig. 8a) of the quadratic form:

$$z = 3x^2 + y^2, \tag{15}$$

the second partial derivatives can be evaluated analytically:

$$\frac{\partial^2 z}{\partial x^2} = 6, \quad \frac{\partial^2 z}{\partial y^2} = 2, \text{ and } \frac{\partial^2 z}{\partial x \partial y} = 0. \tag{16}$$

Using these values to calculate the approximate principal directions of curvature according to thin plate theory one finds $\alpha_1 = 0$, and $\alpha_2 = \pi/2$ everywhere in this basin. The approximate direction of maximum curvature, depicted by tick marks in Fig. 8c, can be compared with the exact maximum curvature direction, λ_1, calculated using Eq. (10) and shown as tick marks in Fig. 8b. Clearly, the constant principal direction obtained assuming the small deflections of plate theory does not closely approximate the changing directions for this basin except along the $x = 0$ axis.

The error in maximum curvature magnitude for this basin is depicted in Fig. 9. The error is defined as:

$$\text{error } [\%] = \frac{k(\lambda_1) - k(\alpha_1)}{k(\lambda_1)} \times 100, \tag{17}$$

where $k(\lambda_1)$ is the exact value and $k(\alpha_1)$ is the approximate value of curvature. Here it can be seen that significant differences between the approximate and exact solution are introduced where the slope of the surface differs from zero. Only near the center of the basin where the slope is small are the errors small. The error exceeds 50% for slopes of approximately 30°. Apparently, using the small deflections of thin plate theory is only valid for surfaces that exhibit very small dips, therefore excluding the application of the approximate equations to many geological surfaces.

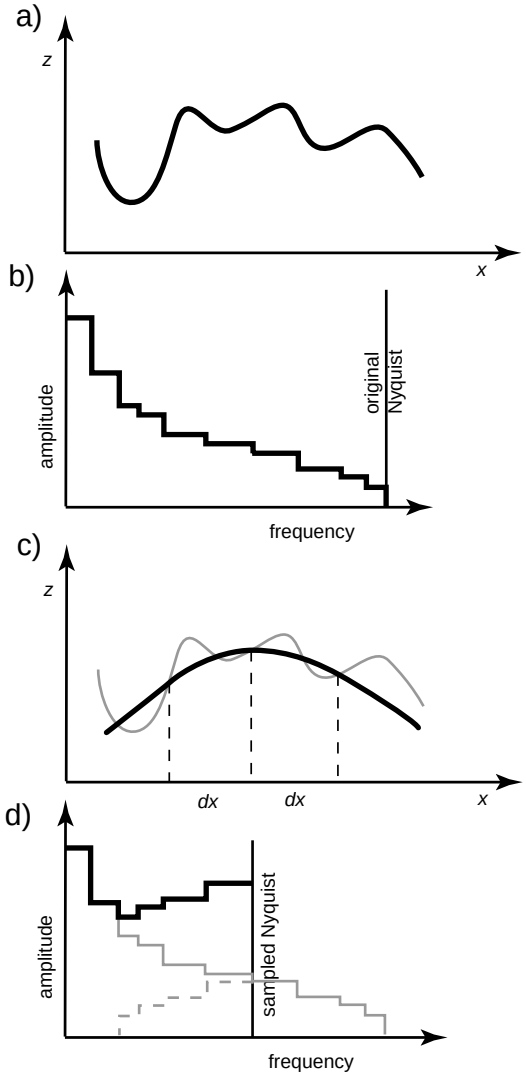

Fig. 10. Aliasing due to discrete sampling of a spatial series. (a) An arbitrary line, and (b) its idealized amplitude/frequency (power) spectrum. Note location of original Nyquist frequency. (c) The aliased representation of the line (heavy line) after re-sampling over a grid with grid-spacing dx. Small undulations of the original (gray) line are not captured in the discretized line representation. (d) Idealized power spectrum after re-sampling. Solid black line depicts the idealized power spectrum of the resampled line. The amplitudes of the frequencies that are not captured by the sampling (to the right of the sampled Nyquist frequency) leaked into the amplitudes of the lower frequencies. The amplitudes of the frequencies of the sampled line are the sum of the original amplitudes (solid gray lines in (d)) plus the amplitudes of the mirror image of the removed amplitudes (dashed gray in (d)).

4.4. Methods for finding principal curvatures

Upon calculating the coefficients of the First and Second Fundamental Forms in the global coordinate system, the normal curvature can be calculated in any direction across the surface by adjusting dx and dy in Eq. (7). For practical applications, the directions and magnitudes of the principal curvatures are commonly of interest, and these can be found analytically using Eqs. (9) and (10). Instead of analytically solving for the principal directions, Lisle and Robinson (1995) and Stewart and Podolski (1998) propose to search numerically for the directions of extreme curvature by including adjacent grid nodes and by using a geometric construct for curvature. Moreover, some investigators simply calculate the structural curvature in 1-D or the curvature according to Eq. (8) along global coordinate lines (the x and y-directions) assuming that these measures of curvature coincide with the directions of principal curvature (e.g. Murray, 1968). It can be seen from inspection of Fig. 8 that the coordinate lines coincide with the directions of principal curvature only at special points. Relying on these or similar simplifications when searching for the principal curvatures should be avoided.

5. The sampling problem

Since analytical expressions for geological surfaces can generally not be established, the horizons usually are represented as depth measurements over a rectangular grid (e.g. seismic or GPS data). Normally, finer grids provide more accurate surface representations, allowing a better resolution of subtle changes of surface attitudes. Surfaces can be approximated using Fourier analysis by a summation of sine and cosine-functions of different frequencies and amplitudes (e.g. Bracewell, 2000). Whereas the low frequencies constitute the broad surface morphology, the high frequency contributions are responsible for the small-scale undulations. The highest frequency contained in a gridded data set is called the Nyquist frequency, which is the inverse of twice the grid spacing. For a sampled surface to be a true representation of the original surface, the Nyquist frequency must equal the frequency of the smallest surface undulation. Sampling a surface at frequencies below its Nyquist frequency introduces an alias, which is the power of the frequencies higher than the sampling frequency leaking into the lower frequencies (Fig. 10). For all practical purposes, a discretized geological surface is thus inevitably aliased with respect to the original surface, and increasingly so for coarser sample grids. In accordance with this inherent sampling problem, surface derivatives and curvature calculated over a sample grid are band-limited, as they only represent a certain range of frequencies. These are aliased representations of the true surface derivatives and curvature.

In order to evaluate the effect of the choice of grid spacing when discretizing surfaces on calculated curvatures, we compare curvature calculated along a sampled line for two different grid spacings (dx) with the curvature calculated from the analytical expression of the line. As shown in Fig. 11, calculated curvatures not only differ significantly for the different grid spacings used, but both estimates depart from the analytical solution. This is true not only in an absolute sense, but also with respect to the locations of the maxima. Moreover, sampling the line at larger intervals increases the sampling alias, and generally underestimates the amplitude of the original line. Therefore, the magnitude

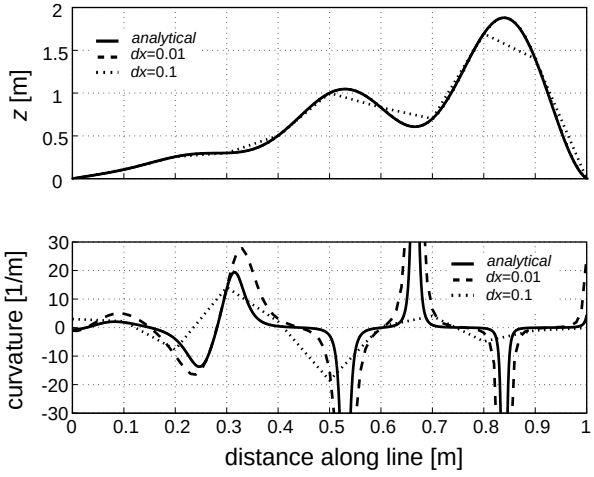

Fig. 11. Effects of discrete sampling on curvature computation. For an arbitrary curved line (solid line, upper), the curvature along the line (lower) is calculated analytically and after re-sampling the line with different grid spacings dx. Compared with the analytical solution, the extreme curvature magnitudes of the sampled (aliased) lines are different for the different grid spacings, and the locations where the curvature assumes extreme values do not coincide. Note that the alias of the curved line increases for increasing grid spacing (upper).

of the resolved curvature decreases (Fig. 11). This implies that the grid spacing gives an upper bound on the value of curvature that can be resolved. This makes curvature analysis over sampled surfaces inherently ambiguous, as the surfaces are likely to contain undulations with greater curvatures. Thus, using surface curvatures to calculate bending strains (e.g. Ekman, 1988; Lisle, 1994; Nothard et al., 1996; Samson and Mallet, 1997; Roberts, 2001) will provide arbitrary strain estimates limited by the sampling grid.

The grid dependency of calculated curvature has been noted by Schultz-Ela and Yeh (1992); however, Stewart and Podolski (1998) treat the problem in more detail. They conclude that calculating curvature using the seismic bin spacing without prior data manipulation will lead to arbitrary curvature values. This can be demonstrated using a curvature analysis performed on the top-Pennsylvanian horizon of the Goose Egg dome, Wyoming (Harris et al., 1960; Lisle, 1994). The top Pennsylvanian is laterally folded into a dome and a saddle as shown in the structure contour map (Fig. 12a). The maximum principal curvature magnitudes and the directions of maximum principal curvature were calculated (Fig. 12b) over the same sample grid used by Lisle (1994). Calculated maximum curvature appears patchy, only hinting at the fact that higher curvature values are observed at the crest of the structure. The curvature contours bear little resemblance to the overall geometry of the surface. Similarly, the maximum curvature changes direction seemingly at random, without showing a clear relation to the dome and saddle geometry.

Fig. 12c depicts the *structural Gaussian* curvature. We refer to *structural Gaussian* curvature as a special case of the Gaussian curvature G: instead of showing

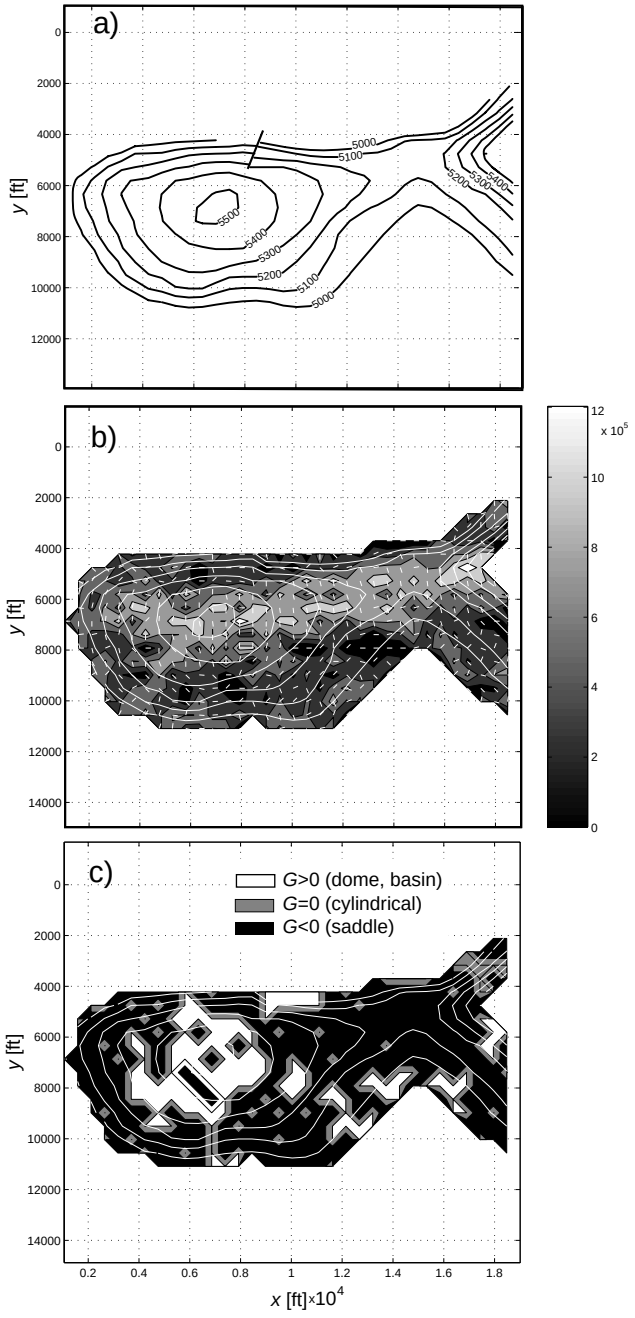

Fig. 12. Curvature analysis of the Goose Egg dome, Wyoming (from Harris et al., 1960) before data manipulation. (a) Structure contour map of the top Pennsylvanian (contour interval: 100 ft). (b) Calculated maximum curvature of the structure before smoothing (absolute magnitudes shown as filled contours), and directions of maximum principal curvature (white ticks). (c) Map of *structural Gaussian* curvature (G): areas where $G<0$ indicating the location of saddle points are shown in black, areas where $G>0$ are depicted in white showing points on domes or basins, and $G=0$ (gray areas) indicating cylindrical points. Calculated mean curvature M (not shown) is positive everywhere. The broad features such as the dome and the saddle that make up the structure are barely resolved by the curvature analysis.

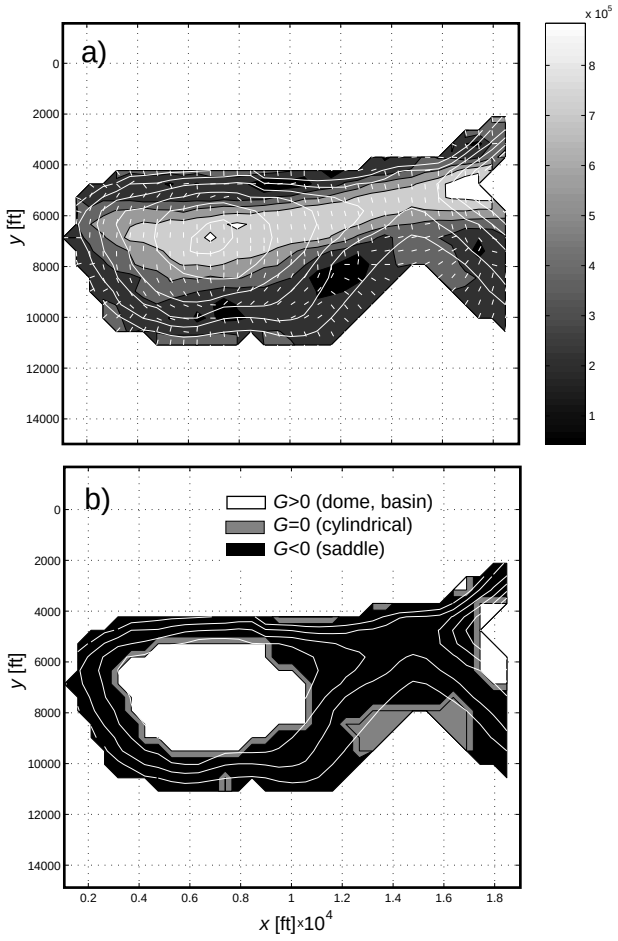

Fig. 13. Curvature analysis of the Goose Egg dome after data smoothing. (a) Calculated maximum curvature for the Goose Egg dome after smoothing (absolute magnitudes shown as filled contours), and directions of maximum principal curvature (white ticks). (b) Map of *structural Gaussian* curvature G of the smoothed data. Calculated mean curvature M (not shown) is positive everywhere. The broad features such as the dome and the saddle that make up the structure are now captured by the curvature analysis.

the absolute value of G we only distinguish positive, negative, and zero Gaussian curvatures. Because the mean curvature (not shown) is positive everywhere, areas of negative Gaussian curvature are shown in black and thus indicate the location of local saddle points (compare with Fig. 5); areas of positive Gaussian curvature are shown in white and represent local domes; and areas of zero Gaussian curvature are shown in gray and depict local cylindrical anticlines. Similar to the results obtained by Lisle (1994, Fig. 8), the apparent large-scale structures that constitute the top Pennsylvanian at Goose Egg dome, i.e. the dome and the saddle, are not resolved by the curvature analysis. The relevance of this and similar curvature analyses (Thomas et al., 1974; Schultz-Ela and Yeh, 1992; Lisle and Robinson, 1995; Ericsson et al., 1998) on raw discretized data is questionable, but the next section shows how this can be improved upon.

6. Data smoothing to improve curvature analysis

In order to add relevance to the calculated curvature of sampled surfaces the calculated curvature necessarily needs to be independent of the grid spacing, meaning that greatest calculated curvatures should not be limited by the choice of grid spacing. As previously suggested by Stewart and Podolski (1998), this can be achieved by separating the higher frequency undulations from the data. Several techniques that can be employed to manipulate a surface such as data decimation, data smoothing, and polynomial fitting are briefly discussed by Stewart and Podolski (1998). Stewart and Wynn (2000) propose calculation of curvature spectra over a range of different grid spacings to capture the range of different curvature wavelengths inherent in the surface data. Investigating the true surface curvature by distinguishing curvatures of different wavelengths is a promising idea. However, the method the investigators propose has a similar effect as data decimation as it increases the sample alias, thus decreasing the accuracy of the true representation of the surface. A subsequent curvature analysis can only be as accurate as the sampled representation of the surface.

We suggest separating high frequency surface undulations from the broad structural content in the data by data smoothing. Because data smoothing is done using the same grid on which the surface was recorded, it thus does not require re-sampling of the surface at larger intervals, and the increase of surface aliasing will be minimized. Theoretically, if a filter effectively removes a certain frequency range with its amplitudes, the resulting surface representation should not suffer more aliasing from this data manipulation.

In order to show the effect of data smoothing on curvature analysis, the Goose Egg dome data (Fig. 12) was smoothed using a low-pass moving average filter. The filter was designed such that it computes an average value for each grid point from the eight nearest data points, weighting all data points equally. The filter moves every data point vertically such that it represents a mean of its eight neighbors, thus smoothing the data as some of the higher frequencies are removed. Aliasing is to be expected even if the filter is applied carefully; however, this effect should be small as this filtering represents a gentle way of manipulating the data. The alias introduced by the data manipulation can be quantified by comparing the structure contours of the original (Fig. 12) and smoothed (Fig. 13) surfaces. As a result of the smoothing procedure the maximum curvature now shows coherent patterns (Fig. 13a), being highest across the crest of the structure, as expected. The directions of maximum curvature (white ticks) trend at high angles to the crest of the structure. The mean curvature is still positive everywhere, and in combination with the structural Gaussian curvature of the smoothed data (Fig. 13b) now clearly resolves the location of the dome (white area) and the saddle (black area). Thus, removing some of the high

frequency content of data has clarified the calculated curvature distribution significantly. If one is interested in the curvature content of the high frequency undulations, a curvature analysis of the removed undulations could be performed.

The choice of technique used to filter the data may produce undesired results; highly effective low-pass filters such as polynomial fitting (Stewart and Podolski, 1998) have the potential to oversimplify the original surface, whereas gentle filters such as the moving average applied here may have a less significant effect on the data. The choice of data manipulating technique will depend on the scale of investigation and the need to remove certain frequencies effectively while minimizing the surface alias. The choice of filter also depends on what surface features one is trying to investigate. If, for example, a curvature analysis of the overall shape of the surface is desired, only the longest wavelengths that make up the surface should be considered, and a low-pass filter would be the obvious choice to smooth the data. A low-pass filter eliminates the high frequencies from the surface data, only allowing the low frequencies to pass. The data can be filtered until coherent and geological sensible surface geometries are extracted.

7. Conclusion

Approximating the normal curvature of a surface either by the second partial derivative or by the curvature of a planar curve leads to erroneous results. Errors in calculated curvature magnitudes exceed 50% on strata folded to dips of about 30°. The locations of extreme curvature values and the directions of the principal curvatures are also likely to be estimated inaccurately using these approximations. Using the technique presented here one calculates normal surface curvature (e.g. principal curvatures and their directions, Gaussian and mean curvature) over sampled surfaces without having to rely on approximations or surface triangulation.

Curvature calculated over a grid is band-limited and thus ambiguous without prior data manipulation, because calculated curvature only represents those surface undulations captured by the sampling grid. The greatest curvature values that can be estimated over a grid are a function of the grid spacing and therefore represent arbitrary upper bounds on the resolvable surface curvature compared with its true curvature content. Strains calculated from the estimated curvatures would suffer from the same arbitrariness. Data manipulation prior to curvature analysis is necessary to ensure that calculated curvatures are independent of the sample grid. We suggest smoothing surface data with a moving average low-pass filter prior to curvature analysis to separate high frequency surface undulations from the broad surface morphology, such that the increase in data alias is small.

Acknowledgements

This research was supported by the Stanford Rock Fracture Project. S. Bergbauer was supported by a Graduate Fellowship from Phillips Petroleum Company. Discussion with T. Mukerji and C. Steele significantly contributed to this research and are greatly appreciated. This paper greatly benefited from comments by J. Evans, P. Geiser, P. Hennings, and S. Stewart.

References

Ames, W.F., 1992. Numerical Methods for Partial Differential Equations. Academic Press, Boston.

Ansell, J.H., Bannister, S.C., 1996. Shallow morphology of the subducted Pacific plate along the Hikurangi margin, New Zealand. Physics of the Earth and Planetary Interiors 93, 3–20.

Bevis, M., 1986. The curvature of Wadati–Benioff zones and the torsional rigidity of subducting plates. Nature 323, 52–53.

Bracewell, R.N., 2000. The Fourier Transform and its Applications. McGraw-Hill, Boston.

Calladine, C.R., 1986. Gaussian curvature and shell structures. In: Gregory, J.A. (Ed.). The Mathematics of Surfaces. Clarendon Press, Oxford, pp. 179–196.

Ekman, M., 1988. Gaussian curvature of postglacial rebound and the discovery of caves created by major earthquakes in Fennoscandia. Geophysica 24, 47–56.

Ericsson, J.B., McKean, H.C., Hooper, R.J., 1998. Facies and curvature controlled 3D fracture models in a Cretaceous carbonate reservoir, Arabian Gulf. In: Jones, G., Fisher, Q.J., Knipe, R.J. (Eds.), Faulting, Fault Sealing and Fluid Flow in Hydrocarbon Reservoirs. Geological Society Special Publications 147, pp. 299–312.

Ewy, R.T., Hood, M., 1984. Surface strain over longwall coal mines; its relation to the subsidence trough curvature and to surface topography. International Journal of Rock Mechanics and Mining Sciences 21, 155–160.

Fischer, M.P., Wilkerson, M.S., 2000. Predicting the orientation of joints from fold shape: results of pseudo-three-dimensional modeling and curvature analysis. Geology 28, 15–18.

Gauss, K.F., 1827. General Investigations of Curved Surfaces, In: Morehead, J.C., Hiltebeitel, A.M. (Trans.), Karl Friedrich Gauss, General Investigations of Curved Surfaces of 1827 and 1825 (published in 1902). The Princeton University Library, Princeton.

Gibbs, A.D., Jaffri, F., Murray, T., 1997. New techniques for fracture distribution and prediction from kinematic modelling of 3D strain fields. AAPG Annual Convention Abstracts.

Harris, J.F., Taylor, G.L., Walper, J.L., 1960. Relation of deformational fractures in sedimentary rocks to regional and local structures. AAPG Bulletin 44, 1853–1873.

Hennings, P.H., Olson, J.E., Thompson, L.B., 2000. Combining outcrop data and three-dimensional structural models to characterize fractured reservoirs: an example from Wyoming. AAPG Bulletin 84, 830–849.

Ivanov, S.S., 1989. Effect of changes in curvature of the surface of the oceanic lithosphere on its stress state. Oceanology 29, 465–468.

Jackson, M.D., Pollard, D.D., 1988. The laccolith-stock controversy; new results from the southern Henry Mountains, Utah. GSA Bulletin 100, 117–139.

Jamison, W.R., 1997. Quantitative evaluation of fractures on Monkshood anticline, a detachment fold in the foothills of Western Canada. AAPG Bulletin 81, 1110–1132.

Johnson, K.M., Johnson, A.M., 2000. Localization of layer-parallel faults in San Rafael swell, Utah and other monoclinal folds. Journal of Structural Geology 22, 1455–1468.

Lisle, R.J., 1992. Constant bed-length folding: three-dimensional geometrical implications. Journal of Structural Geology 14, 245–252.

Lisle, R.J., 1994. Detection of zones of abnormal strains in structures using Gaussian curvature analysis. AAPG Bulletin 78, 1811–1819.

Lisle, R.J., Robinson, J.M., 1995. The Mohr circle for curvature and its application to fold description. Journal of Structural Geology 17, 739–750.

Mallet, J.L., 1992. Discrete smooth interpolation in geometric modelling. Computer Aided Design 24, 178–191.

Murray, G.H., 1968. Quantitative fracture study-Sanish Pool, McKenzie County, North Dakota. AAPG Bulletin 52, 57–65.

Nothard, S., McKenzie, D., Haines, J., Jackson, J., 1996. Gaussian curvature and the relationship between the shape and the deformation of the Tonga slab. Geophysical Journal International 127, 311–327.

Nutbourne, A.W., Martin, R.R., 1988. Differential Geometry Applied to Curve and Shell Design. Ellis Horwood Limited, Chichester.

Pollard, D.D., Johnson, A.M., 1973. Mechanics of growth of some laccolithic intrusions in the Henry Mountains, Utah; II. Bending and failure of overburden layers and sill formation. Tectonophysics 18, 311–354.

Roberts, A., 2001. Curvature attributes and their application to 3D interpreted horizons. First Break 19, 85–100.

Samson, P., Mallet, J.-L., 1997. Curvature analysis of triangulated surfaces in structural geology. Mathematical Geology 29, 391–412.

Schultz-Ela, D.D., Yeh, J., 1992. Predicting fracture permeability from bed curvature. Proceedings—Symposium on Rock Mechanics, Santa Fe, NM.

Stewart, J., 1995. Multivariable Calculus. Brooks/Cole Publishing Company, Pacific Grove.

Stewart, S.A., Podolski, R., 1998. Curvature analysis of gridded surfaces. In: Coward, M.P., Daltaban, T.S., Johnson, H. (Eds.), Structural Geology in Reservoir Characterization. Geological Society Special Publications 127, pp. 133–147.

Stewart, S.A., Wynn, T.J., 2000. Mapping spatial variation in rock properties in relationship to scale-dependent structure using spectral curvature. Geology 28, 691–694.

Stoker, J.J., 1969. Differential Geometry. John Wiley & Sons, New York.

Struik, D.J., 1961. Lectures on Classical Differential Geometry. Addison-Wesley Publishing Company, London.

Thomas, A., Mallet, J.L., De Beaucourt, F., 1974. An analytic method for localizing structural discontinuities in a rock mass. Proceedings of the Congress of the International Society for Rock Mechanics.

Timoshenko, S., Woinowsky-Krieger, S., 1959. Theory of Plates and Shells. McGraw-Hill, New York.

Turcotte, D.L., Schubert, G., 1982. Geodynamics; Applications of Continuum Physics to Geological Problems. John Wiley & Sons, New York.